


Coalescence-induced droplet spreading: Experiments aboard the International Space Station

Cite as: Phys. Fluids **34**, 122110 (2022); <https://doi.org/10.1063/5.0125279>

Submitted: 10 September 2022 • Accepted: 28 September 2022 • Accepted Manuscript Online: 30 September 2022 • Published Online: 13 December 2022

 J. McCraney,  J. Ludwicki,  J. Bostwick, et al.

COLLECTIONS

 This paper was selected as Featured



View Online



Export Citation



CrossMark

ARTICLES YOU MAY BE INTERESTED IN

[Air-in-liquid compound drop impact onto a pool](#)

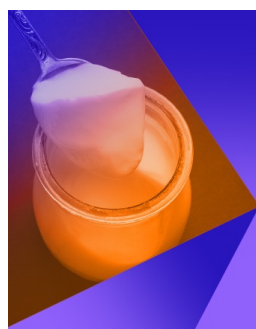
Physics of Fluids **34**, 102101 (2022); <https://doi.org/10.1063/5.0086745>

[Enhanced horizontal mobility of a coalesced jumping droplet on superhydrophobic surfaces with an asymmetric ridge](#)

Physics of Fluids **34**, 122104 (2022); <https://doi.org/10.1063/5.0121402>

[Drop impact dynamics on solid surfaces](#)

Applied Physics Letters **121**, 210501 (2022); <https://doi.org/10.1063/5.0124256>



Physics of Fluids

Special Topic: Food Physics

Submit Today!

Coalescence-induced droplet spreading: Experiments aboard the International Space Station

Cite as: Phys. Fluids **34**, 122110 (2022); doi: [10.1063/5.0125279](https://doi.org/10.1063/5.0125279)

Submitted: 10 September 2022 · Accepted: 28 September 2022 ·

Published Online: 13 December 2022



View Online



Export Citation



CrossMark

J. McCraney,^{1,a)}  J. Ludwicki,¹  J. Bostwick,²  S. Daniel,¹  and P. Steen¹ 

AFFILIATIONS

¹Robert Frederick Smith School of Chemical and Biomolecular Engineering, Cornell University, Ithaca, New York 14853, USA

²Department of Mechanical Engineering, Clemson University, Clemson, South Carolina 29631, USA

^{a)} Author to whom correspondence should be addressed: jm2555@cornell.edu

ABSTRACT

We report experiments of centimeter-sized sessile drop coalescence aboard the International Space Station, where microgravity conditions enable inertial-capillary spreading motions to be explored for a range of hydrophobic wetting conditions. Observations of the time traces of the coalescence event and projected areas compare favorably to numerical simulations, which employ the Davis–Hocking contact line (CL) condition with contact line mobility M parameter independently measured using the resonant-frequency scan technique of Xia and Steen [“Moving contact-line mobility measured,” J. Fluid Mech. **841**, 767–783 (2018)]. This observation suggests that M is a material parameter, and that the Davis–Hocking model is an appropriate CL model for inertial-capillary spreading.

Published under an exclusive license by AIP Publishing. <https://doi.org/10.1063/5.0125279>

I. INTRODUCTION

Coalescing drops are prominent in rainwater runoff from building facades,¹ cell–cell interaction and cell adhesion to biological tissues,² condensing steam for energy generation,³ thermal management of electronic components,⁴ self-cleansing surfaces,⁵ electrowetting,⁶ among others. While knowledge of the liquid viscosity and surface tension is sufficient to describe the dynamics of freely suspended coalescing drops, the solid–liquid–gas line of contact [contact line (CL), dashed line in Fig. 1(a)] modulates the dynamics of sessile drops.^{7–9} Here, inertial-capillary spreading can occur over short time scales, as defined by the competition between inertia and surface tension forces, making sessile drop coalescence an excellent system to study such motions. To improve modeling and predictive capabilities for coalescing sessile drops, high spatial and temporal resolution experiments are paramount, yet lacking,¹⁰ because on Earth spreading occurs over small length scales and fast time scales (drops coalesce within a millisecond¹¹). Here, we exploit the large drop sizes possible on the International Space Station (ISS) to study inertial-capillary spreading. For water in air, the terrestrial capillary length $\ell_c = \sqrt{\sigma/\rho g} \approx 3$ mm, with σ the surface tension, ρ the density, and g the gravitational acceleration. In contrast, on the ISS, $\ell_c \approx 3$ m or roughly up to three orders of magnitude larger than on Earth. This allows for experimentation of much larger drops with correspondingly slower time scales, thereby

extending the experimental parameter space for sessile drop coalescence. Previous terrestrial studies examine droplet coalescence at Reynolds numbers $Re \sim \mathcal{O}(10^2)$ and Ohnesorge numbers $Oh \sim \mathcal{O}(10^{-3})$.^{12,13} With the ISS advantage, we report experiments in a regime where Reynolds numbers are an order of magnitude larger, and Ohnesorge numbers are an order of magnitude smaller than prior work, thereby extending the overall parameter range with which hydrophobic water droplet coalescence is studied.

Our interest is in water under hydrophobic wetting conditions, Fig. 1(a), where wall dissipation is limited and two demarcated flow regimes are observed:^{14,15} capillary-inertial and capillary-viscous. Due to the prevalence of inertial-capillary coalescence in real-world applications on hydrophobic surfaces (i.e., optimizing the heat transfer coefficient via dropwise condensation,¹⁶ spray cooling,^{17,18} and ink-jet printing^{19,20}), the focus of our study is on the inertial-capillary regime, which we briefly describe referring to the experiment shown in Fig. 2, where after coalescence, the droplet spreads toward equilibrium. Initially, two drops rest in equilibrium, evidenced by the constant interface curvatures. Upon coalescence ($t = 0.03$ s), an immediate curvature gradient is observed at the liquid bridge, which induces a pressure gradient according to the Young–Laplace equation that gives rise to a capillary wave propagating laterally across the bridge.²¹ This process continues until $t = 0.24$ s, at which point surface tension

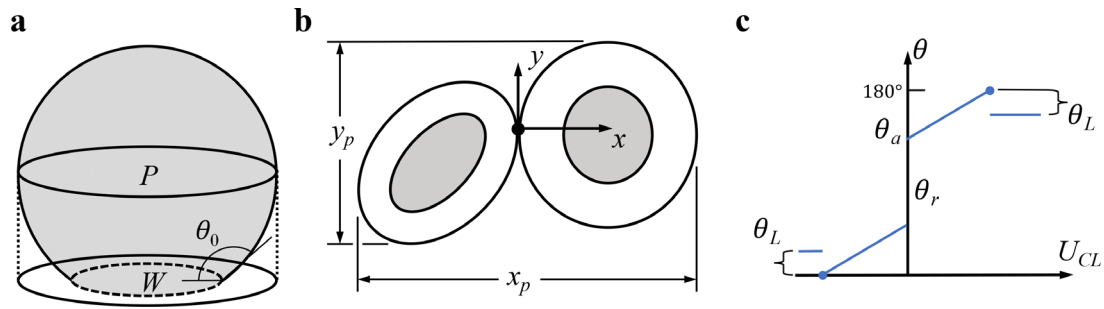


FIG. 1. (a) Schematic of sessile drop with initial contact angle $\theta_0 > 90^\circ$, showing projected P and wetted W contact areas. (b) Projected (top) view of coalescing sessile drops with coordinate system overlaid and maximal projected x - and y -distances denoted x_p and y_p . (c) Davis–Hocking relating the contact angle θ to the CL velocity U_{CL} with θ_a and θ_r , the static advancing and receding contact angles, respectively.

overwhelms inertia and the drop CL begins to recede. This competition between inertia and capillarity continues until a sufficient amount of energy is dissipated via CL motions, at which point the CL is pinned ($t = 0.63$ s). The inertial-capillary flow that occurs as the droplet spreads toward equilibrium is described by a large Reynolds number $Re \gg 1$ and small capillary number $Ca \ll 1$ with negligible viscous effects. This is a distinguished regime from most studies of spreading, which is slow and often characterized as a visco-capillary flow.

In any study of spreading, the contact line physics is of paramount importance. Several continuum contact line laws have been advanced,²² modeling the liquid as a continuous media and prescribing CL behavior accordingly. Of particular interest to this work is the Davis–Hocking model^{23,24} of CL motion,

$$M\Delta\theta = U_{CL}, \quad (1)$$

which relates the difference in contact angle from its equilibrium value $\Delta\theta = \theta - \theta_0$ to the contact line velocity U_{CL} through the CL mobility parameter M , which has previously been viewed as CL resistance $1/M$.²⁵ We note the Davis–Hocking model employed herein is a macroscopic continuum approximation of the complex molecular dynamics (MD) underpinning the CL process.²⁶ However, the computational expense of MD models remains extensive. While progress toward continuum-MD hybrid simulations shows promise,^{27,28} the CL physics remains elusive, though innate in droplet-spreading phenomena.²⁹ For these reasons, our interest in the Davis–Hocking law lies in its simplicity and computational affordability. However, one challenge with

implementing the Davis–Hocking model is determining M , which has historically been determined as a numerical fitting parameter. However, a recent breakthrough by Xia and Steen³⁰ introduced a technique to experimentally measure M by a resonant frequency sweep of sessile drop motions. Here, we test whether M is a material parameter by using the technique of Xia and Steen to measure M , which can then be input as a known parameter into numerical simulations of sessile drop coalescence that are then compared with experiment. We show that numerical simulation compares favorably to experiment, suggesting that the Davis–Hocking model is an appropriate CL law for inertial-capillary spreading, and that M can be viewed as a material parameter (functions solely of CL velocity and contact angle) in this context.

II. METHODS

A. Experiment

Sessile water drop coalescence experiments were performed on four hydrophobic surfaces (S_1 , S_2 , S_3 , and S_4) in microgravity conditions aboard the ISS. All substrates are made of Teflon and sanded to various degrees to produce the associated wetting properties shown in Table I. Surface wetting properties were measured first on Earth, though material degradation was expected due to transport and storage from terrestrial to ISS lab. All measured parameters degraded within 10% of their terrestrial-measured values. As such, all experimental and simulated quantities reported in Table I were measured aboard the ISS from a side view PixeLINK PL-D674MU camera at

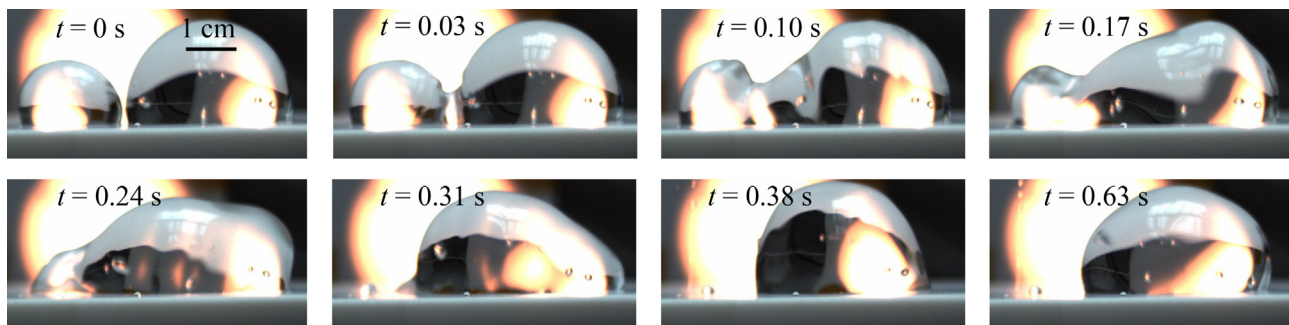


FIG. 2. Side perspective of drop coalescence event on S_1 surface from initial profile $t = 0$ s up to CL pinning $t = 0.63$ s. The apparent “snow-caps” atop the drops are substrate-edge reflections from the rear viewing light, which are exaggerated by the massive drop size.

TABLE I. Substrate identification table with corresponding wetting properties: static, advancing, and receding contact angles of θ_0 , θ_a , and θ_r , respectively, hysteresis $\Delta\theta_H \equiv \theta_a - \theta_r$, pre-positioned drop radius R and mobility parameter M . All angles within $\pm 2^\circ$ error.

ID	Substrate	$\theta_0(^{\circ})$	$\theta_a(^{\circ})$	$\theta_r(^{\circ})$	$\Delta\theta_H$	R (cm)	M (m/s rad)
S_1	Unsanded	115	116	77	39	1.62	0.23
S_2	320 grit sanded	130	155	100	55	1.55	0.19
S_3	240 grit sanded	143	163	62	101	1.63	0.09
S_4	120 grit sanded	128	148	59	89	1.40	0.12

50.5 fps. To accurately measure these wetting quantities, a single drop (no coalescence) was placed on the substrate mounted to a shaker table and oscillated in the plane-normal direction at the first resonant frequency (approximately 2 Hz for all surfaces).^{25,31} This induces large advancing and receding CL motions, as shown in Figs. 3(a) and 3(b) from which the advancing θ_a and receding θ_r contact angles were measured by curve fitting a line to the CL edge of the binary images 3(c) and 3(d). Static contact angles θ_0 were measured by fitting a circle to the drop at rest and computing the angle of intersection with the circle and the substrate. The pixel length of the images implies all angles measured have maximum $\pm 2^\circ$ error. The mobility M values were

TABLE II. Fluid properties for water and air (subscript g).

ρ (kg/m ³)	ρ_g (kg/m ³)	μ (mPa s)	μ_g (mPa s)	σ (J/m ²)
998.0	1.204	0.998	0.0181	0.072

measured via the method of Xia and Steen,³⁰ as determined through an experimentally determined relationship between the contact angle deviation from static contact angle θ_0 and contact line velocity U_{CL} . Deionized water was used as the working liquid with properties given in Table II.

Each experiment began by depositing a pre-positioned liquid drop on the substrate via a syringe. A second drop was grown near the pre-positioned first drop until coalescence at $t = 0$, as shown in the top row of Fig. 4. Drop growth was controlled by one of two methods. The first was performed on surfaces S_1 , S_3 , and S_4 , in which the second drop grew in volume by pumping liquid through a hole in the substrate until it coalesced with the pre-positioned drop. The second method was performed on surface S_2 where the astronaut deposited the second drop with a syringe and carefully guided it toward the pre-deposited drop via the syringe, Fig. 4(b). In all cases, care was taken to impose a minimal impact velocity at the coalescence event, although the non-spherical shape of the second deposited drop implies

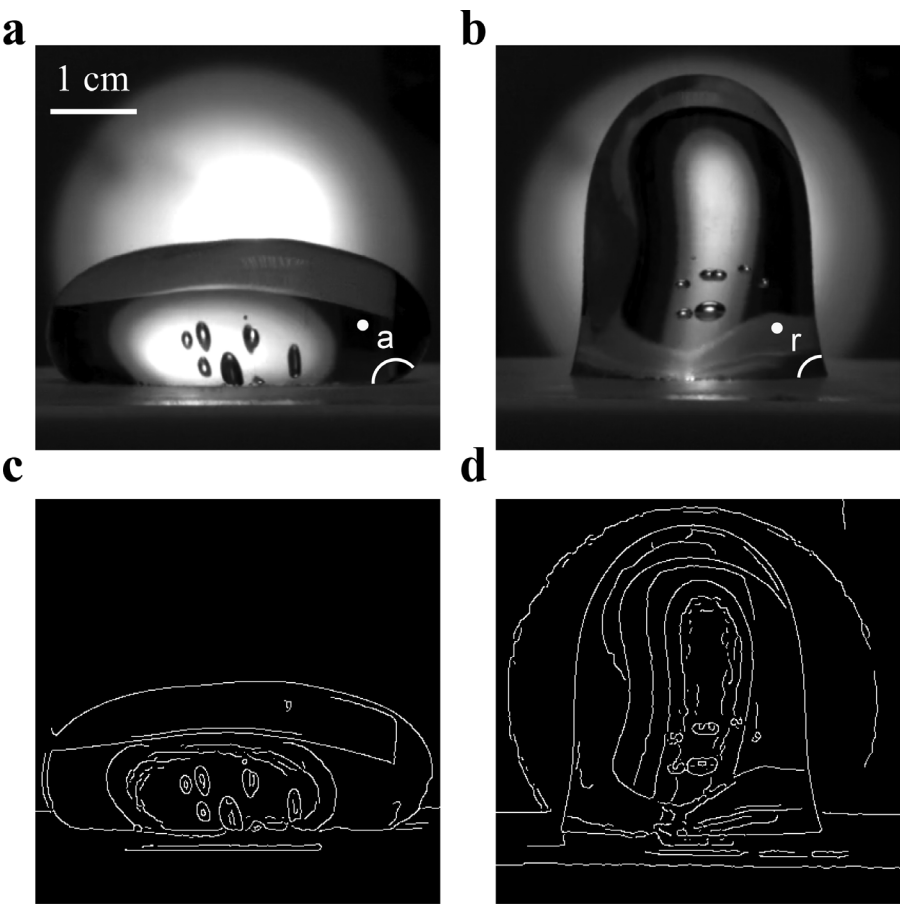


FIG. 3. Resonant droplet motions were used to measure the wetting properties on the ISS, as described by the advancing (a) and receding (b) CLs with (c) and (d) corresponding image edge detection for surface S_3 .

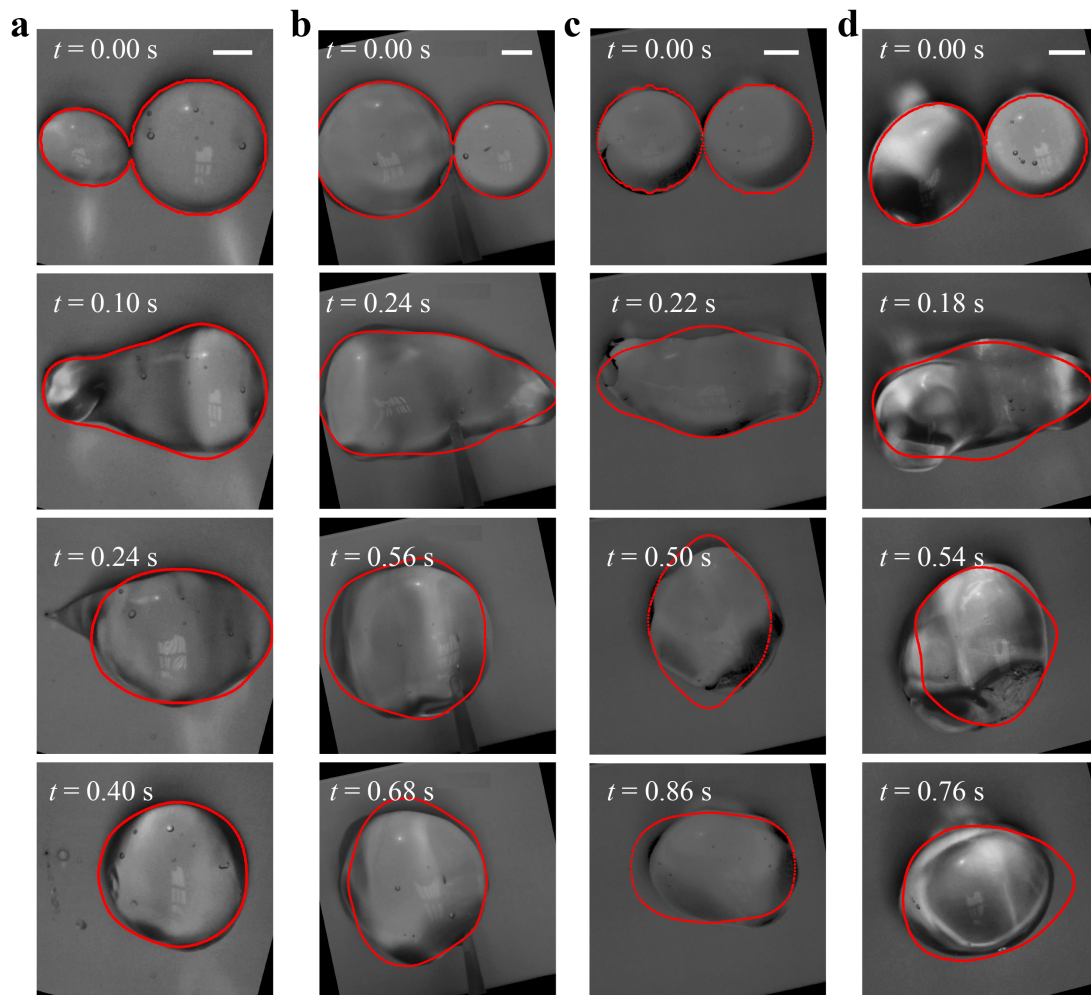


FIG. 4. Time evolution of coalescence in top view overlaid with simulation (red) projections for surfaces (a) S_1 , (b) S_2 , (c) S_3 , and (d) S_4 . All scale bars are 1 cm.

pre-coalescent dynamics, as shown in Figs. 4(a) and 4(d). The experiments were visualized in top and side views by PixelINK PL-D674MU and MSG GiGE 1050 cameras at 50.5 and 28.5 fps, respectively.

Image processing was performed using in-house developed automated interface tracking algorithms to resolve the interface position.^{32,33} To summarize the procedure, we first perform a low-loss conversion of the video to still images files. The images are then further reduced to black-and-white binary files. To reduce image noise due in part to small sparse air bubbles and spurious reflections, we apply a Canny³⁴ filter applying two thresholds for edge detection sensitivity. We then increment the region of interest for each image and tabulate the desired interface pixels. This process is performed many hundreds of times for thousands of pixels for each still frame to resolve the interface position.

B. Numerical simulations

The OpenFOAM computational fluid dynamics software is employed to simulate sessile drop coalescence for the specific

experiments described above. This is important to evaluate the Davis–Hocking model with no fit parameters. We briefly describe the procedure. Pre-processing is specified via blockMesh, a native OpenFOAM stencil tool, here used to generate a $6 \times 6 \times 6 \text{ cm}^3$ cubic computational domain comprised of uniform cubic cells with edge length $\epsilon = 0.5 \text{ mm}$. Increasing cell count by 25% yields less than 1% change in horizontal and vertical coalescence extensions; then, the simulations are considered spatially converged with the chosen ϵ . Initial conditions are specified via the funkySetFields utility, which analytically specifies the initial cell value to a liquid or gas phase. Initial drop shapes were not always spherical [Figs. 4(a) and 4(d)]. For these initial conditions, initial drop shape was determined by fitting ellipsoids to the images, where both the side view (Fig. 2) and top view perspectives enabled fully resolved 3D non-spherical droplet shapes. Drop diameters D , static contact angles θ_0 (cf. Fig. 1), and parameters θ_a , θ_r , and M are taken from experimentally measured values. Fluid properties are given in Table II. Open-flow boundary conditions, i.e., fixed pressure and zero velocity gradient, are specified on all boundaries except the substrate. The gravity vector $\mathbf{g} = 0$, conforming to ISS

TABLE III. Relevant non-dimensional numbers for experiments (subscript E) and simulations (subscript S): Reynolds number $Re = \rho_l U_{CL} D / \mu_l$, capillary number $Ca = \mu_l U_{CL} / \sigma_{lg}$, and Ohnesorge number $Oh = \mu_l / \sqrt{\rho_l \sigma_{lg} D}$, where $D = 2R$ and R is the radius of the pre-positioned drop. Here, U_{CL} is the maximum magnitude of CL velocity on the x -axis.

Substrate	Re_E	Re_S	Ca_E	Ca_S	Oh
S_1	6.55×10^3	5.77×10^3	2.80×10^{-3}	2.46×10^{-3}	6.5×10^{-4}
S_2	5.75×10^3	4.34×10^3	2.57×10^{-3}	1.92×10^{-3}	6.7×10^{-4}
S_3	3.94×10^3	8.73×10^3	1.67×10^{-3}	3.71×10^{-3}	6.5×10^{-4}
S_4	5.80×10^3	3.60×10^3	2.87×10^{-3}	1.78×10^{-3}	7.0×10^{-4}

conditions. Material advection, momentum, and continuity equations are solved for the Davis–Hocking contact angle model, originally developed in OpenFOAM by Ludwicki and Steen.¹² Specifically, we model the contact angle θ as

$$\text{For } U_{CL} \geq 0: \theta = \theta_a + U_{CL}/M \text{ if } \theta \leq 180^\circ, \\ \text{otherwise } \theta = 180^\circ - \theta_L, \quad (2)$$

$$\text{for } U_{CL} < 0: \theta = \theta_r + U_{CL}/M \text{ if } \theta \geq 0^\circ, \text{ otherwise } \theta = \theta_L.$$

to accommodate systems with contact angle hysteresis, with θ_a and θ_r the advancing and receding contact angles, respectively, as shown in Fig. 1(c), and $\theta_L = 5^\circ$ restricts the numerical model from implementing nonphysical contact angle values. We note numerically that a $\pm 5\%$ change in M yields $< 2\%$ change in x_p and y_p extensions, and a $\pm 50\%$ change in M yields $< 15\%$. The contact angle model effectively prescribes the gradient of the cell volume fraction α according to the contact angle. Briefly, before the interface curvature is calculated, the interface normal at the wall boundary is corrected to comply with the target contact angle θ , satisfying $\hat{n}_w \cdot \hat{n}_i = \cos \theta$ at the contact line, where \hat{n}_w and \hat{n}_i are the unit normals of the wall and interface, respectively. Further details of the contact angle implementation are described in detail by Kunkelmann (Ref. 35, Sec. 3.2.4). The numerical solution is computed via *interFoam*, a volume of fluid (VOF) solver, applicable to incompressible, laminar, and two-phase fluid flow. Here, we note that the *interFoam* solver has been modified to remove artificial anti-diffusive surface fluxes, which have been

previously shown to improve transient behaviors in capillary-dominated flows.³⁶ All post-processing is conducted in ParaView, a native software included with the OpenFOAM installation. The relevant non-dimensional numbers for the simulations are given in Table III and are consistent with the inertial-capillary spreading regime, $Re \gg 1$, $Ca \ll 1$, and $Oh \ll 1$, for all cases.

III. RESULTS

Experimentally, two drops coalesce by molecular adhesion, evidenced by a topological change from two distinct bodies of liquid to one. At this instance $t = 0$, a liquid bridge is formed between the two drops, as shown in Fig. 2, which dynamically evolves within the inertial-capillary regime. During this time, two primary curvatures are observed, which include (1) the bulk curvature of the drops with associated positive pressure due to the convex interface and (2) the bridge curvature with negative pressure due to the concave interface. This pressure difference induces large velocity gradients, which lead to recoil of one or both droplets with associated interface deformations. For unequal sized drops, the smaller drop recoils, with minimal CL motions exerted from the larger drop [cf. Figs. 2, 4(a), 4(b), and 4(d)]. Binary drop coalescence exhibits near symmetric recoils of both bulks, Fig. 4(c), and thereby larger CL motions from both drops. Here, projected area swept extensions for binary drops [Fig. 5(c)] exceed those of asymmetric drop coalescence, Figs. 5(a), 5(b), and 5(d).

Hydrophobic wetting conditions combined with the asymmetric nature of coalescence preclude velocity measurements along the entire CL.

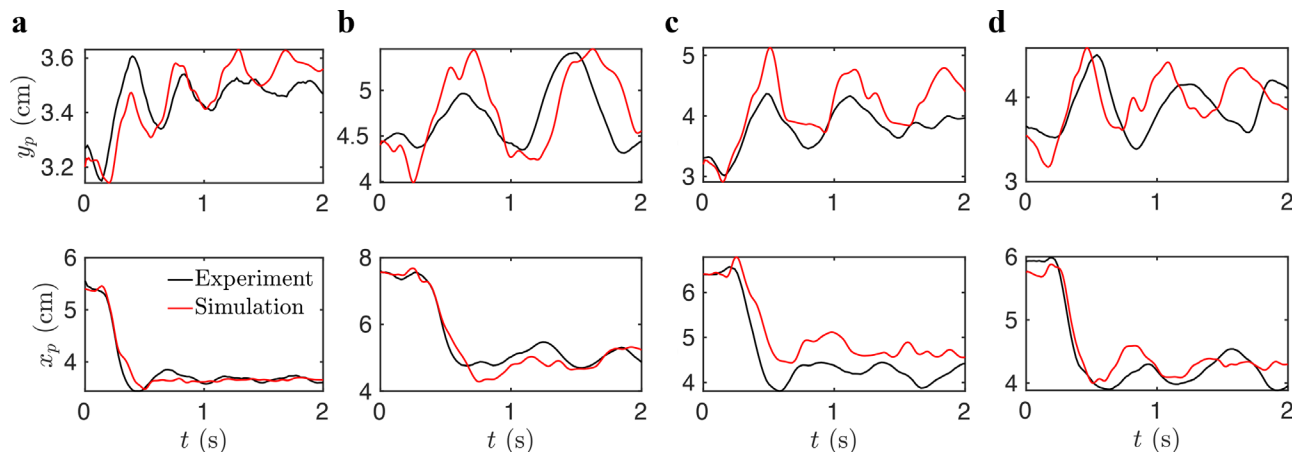


FIG. 5. Time evolution of projected maximal vertical y_p (top row) and horizontal x_p (bottom row) extensions contrasting experiment (black) with simulation (red) for surfaces (a) S_1 , (b) S_2 , (c) S_3 , and (d) S_4 .

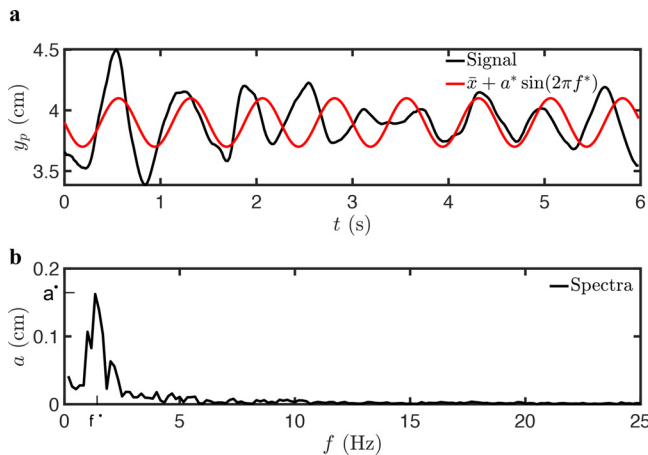


FIG. 6. (a) Raw signal for y_p extension (black) overlaid with a sinusoid at dominant frequency f^* (red), of which the spectra are shown in (b) for surface S_4 .

As such, we quantify the coalescence dynamics through (1) time evolution of the top/side view images and (2) time traces of the maximal horizontal x_p and vertical y_p projected extensions, as shown in Fig. 1(b). Our focus is on the inertial-capillary regime, which occurs during the first half second ($S_{1-4} = 0.63, 0.5, 0.52, 0.52$ s), and ignores the dynamics in the visco-capillary regime, which can last in excess of 40 s. We focus on comparing simulations to experiment to validate the use of the Davis–Hocking CL model. In what follows, we discuss the accuracy of simulations by comparing experiments. Accuracy is assessed via two metrics: (i) qualitative accuracy via time evolution of top perspective coalescence event (cf. Fig. 4) and (ii) quantitative accuracy via time traces of the maximal projected coalescence extensions in the x - and y -axes, $x_p(t)$ and $y_p(t)$, respectively, as shown in Fig. 1(b).

Simulations more accurately model lower hysteresis $\Delta\theta_H \equiv \theta_a - \theta_r$ surfaces S_1 and S_2 as evidenced by Figs. 4(a) and 4(b). This expected result was observed in recent literature on terrestrial-based experiments.¹³ Figure 5 plots the projected extensions x_p and y_p for all surfaces. The simulations most accurately predict early time x_p

extensions during initial coalescence. This is expected, as the coalescence event initiates with horizontal touching, where the small curvatures at horizontal endpoints relative to the large curvatures along the droplet length induce large pressure gradients via the Young–Laplace equation (Fig. 4, second row). These large pressure gradients force the drop to quickly recede to a sphere, thereby increasing inertia. The Davis–Hocking model is found to accurately predict extensional oscillations as determined by performing a fast Fourier transform of the y_p and x_p extensions. Figure 6(a) plots the y_p extension (black) for substrate S_4 for a long time duration of 6 s. Applying a fast Fourier transform of the signal $\bar{x} + a \sin(2\pi f^* t)$ with \bar{x}, a the average extension and maximum amplitude, respectively, for frequency f^* , we can extract the fundamental oscillation frequencies of x_p and y_p extensions from the power spectra shown in Fig. 6(b). Applying this to both simulation and experimental extensions, we find the average simulation oscillation frequency is within 6%–16% of the experimental value for all substrates.

Finally, the liquid bridge evolution was analyzed, and the radius is shown in Fig. 7. *A priori* predictions³⁷ and posteriori measurements^{21,38} have found r_m grows proportional to $t^{0.5}$ for free drop–drop coalescence. We might expect our results to deviate from these predictions, given the wetting effects inherent in sessile drop coalescence. Figure 8 plots the temporal bridge thickness r_m against time for all four surfaces. Perhaps surprisingly, despite the asymmetries in droplet size, shape, and variability of induced coalescence, we find r_m scales as $t^{0.4}$, which is relatively close to the 0.5 exponent and consistent with prior experimental studies that observed exponents ranging from 0.41 to 0.55.³⁹

Simulation and experimental disagreement can be attributed to several unintended factors. In experiment, pre-coalescence dynamics are evident and clearly seen by the ellipsoid projections on surfaces S_1, S_4 , Figs. 4(a) and 4(d). Drop connection to the exit hole results in increased injected liquid volume for substrates S_1, S_3, S_4 , visually shown in Fig. 4(a), $t = 0.24$ s. Given the short time scales and large drops, this added volume should be minimal. Surface S_2 undergoes syringe interference throughout coalescence [Fig. 4(b)], which induces circulation into the drop. All experiments were observed to undergo vibrational asymmetric disturbances, which induce non-negligible

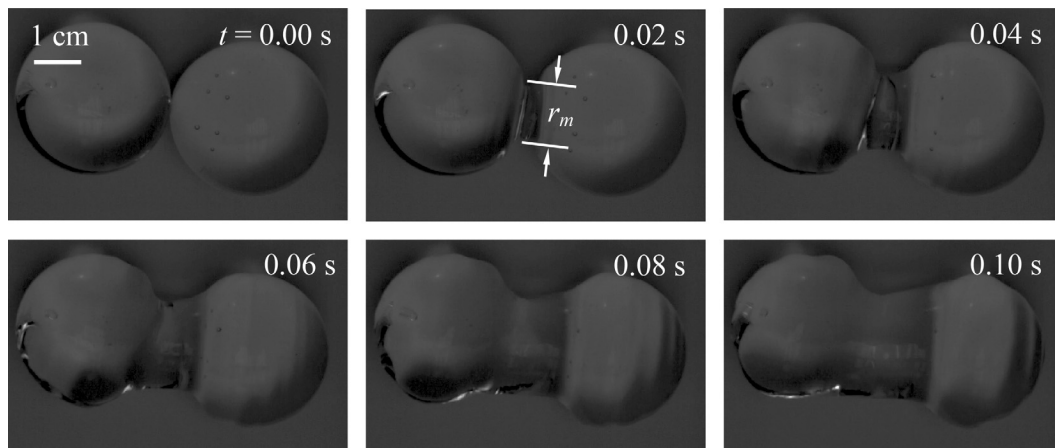


FIG. 7. Top view time evolution of drop coalescence for the S_3 substrate, with neck thickness r_m .

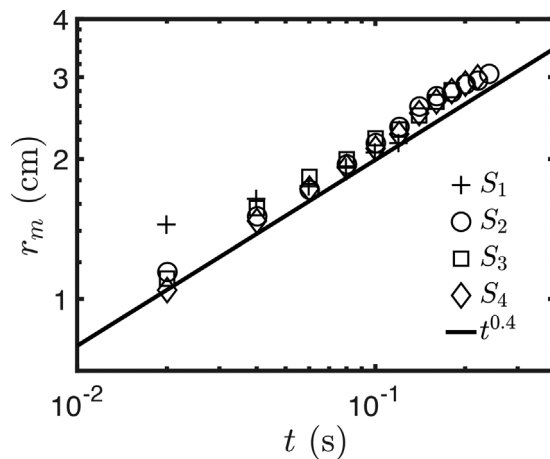


FIG. 8. Liquid bridge thickness r_m against time displays a power law dependence $t^{0.4}$.

rotation, a phenomenon that is initially overcome by the heightened inertia from initial coalescence but impacts system behavior at times $t \geq 0.5$ s. During coalescence, all experiments exhibit spurious air bubbles, many of which are present pre-coalescence, refer to Fig. 4. These air bubbles were not simulated and could impact dynamics. Despite these limitations, the simulations do well to predict droplet coalescence of large drops in microgravity, validating both the Davis–Hocking CL boundary condition and the mobility M measurement.

IV. CONCLUSION

In this work, we reported experiments of sessile drop coalescence under microgravity conditions aboard the ISS. This rare flight data allowed us to access inertial-capillary spreading motions, which are difficult to analyze on Earth due to the short timescale transients and small length scale displacements of the liquid–solid–gas CL. The microgravity conditions allow for experimentation with larger length scales and correspondingly slower time scales, thus enlarging the inertial-capillary spreading regime. With the ISS advantage, we determined the contact line mobility M is a material parameter through the following procedure. First, we experimentally measure M for a given solid–liquid–gas configuration via plane normal surface vibrations of a sessile drop, in this case reported in detail in Xia and Steen³⁰ and use this value of M to model another flow of interest, invoking the Davis–Hocking model without any fit parameters. Here, we use computational fluid dynamics simulations to compare with sessile drop coalescence experiments on four separate hydrophobic substrates. Despite several irregularities among experiments, the Davis–Hocking boundary condition, with experimentally measured M , did well to predict the evolution of the sessile drop coalescence experiments, suggesting, indeed, that M is a material parameter, at least for the flow conditions considered here.

This work elucidates inertial-capillary spreading of a pair of coalescing wall-bound droplets. The results validate the widely accepted liquid bridge evolution prediction of Eggers *et al.*³⁷ in a parameter space never before studied. The reported experiments assume substrates with uniform wetting properties, although, in practice, equilibrium contact angles and CL dynamics can vary even on a single surface, as in wettability-gradient surfaces. Future studies that

investigate the effects of contact angle mismatch on sweeping would be of value. Additionally, CL dynamics need not be isotropic,⁴⁰ which suggests there may be an advancing M_a and receding M_r mobility parameter. Future work in analyzing advancing and receding mobility parameters could lead to a more accurate CL boundary condition for numerical analysts. Additionally, the sweeping behavior of three or more drops with or without chain-reaction coalescence remains unexplored. Open questions persist as to how the number of drops and their positioning affect coalescence sweeping. Finally, a parametric study of contact angle hysteresis would be of benefit to parse whether the equilibrium contact angle or hysteresis is the dominant parameter in determining the extent of coalescence-induced sweeping.

ACKNOWLEDGMENTS

This work was financially supported by the NSF under Award No. 1637960. J.M. acknowledges partial support through the NASA under Grant No. 80NSSC19K0406. J.M.L. also acknowledges support through the NASA Space Technology Research Fellowship program, Award No. 80NSSC17K0144. The authors thank Glenn Swan for fabrication support, and Vanessa Kern for experimental assistance. The authors also thank the ISS astronaut crews—in this case, NASA astronauts Kathleen Rubins and Michael Hopkins for their patience and insight in performing the experiments. We dedicate this work to Paul Steen (1952–2020).

AUTHOR DECLARATIONS

Conflict of Interest

The authors have no conflicts to disclose.

Author Contributions

Joshua McCraney: Data curation (lead); Formal analysis (lead); Methodology (lead); Software (lead); Validation (lead); Visualization (lead); Writing – original draft (lead); Writing – review & editing (equal). **Jonathan Michael Ludwicki:** Conceptualization (supporting); Investigation (supporting); Resources (supporting); Supervision (supporting); Writing – review & editing (equal). **Joshua Bostwick:** Project administration (equal); Supervision (equal); Writing – review & editing (lead). **Susan Daniel:** Funding acquisition (lead); Project administration (equal); Supervision (equal); Writing – review & editing (equal). **Paul Steen:** Conceptualization (lead); Funding acquisition (lead).

DATA AVAILABILITY

The data that support the findings of this study are available from the corresponding author upon reasonable request.

REFERENCES

- B. Blocken, D. Derome, and J. Carmeliet, “Rainwater runoff from building facades: A review,” *Build. Environ.* **60**, 339–361 (2013).
- S. Karpitschka, A. Pandey, L. A. Lubbers, J. H. Weijs, L. Botto, S. Das, B. Andreotti, and J. H. Snoeijer, “Liquid drops attract or repel by the inverted Cheerios effect,” *Proc. Natl. Acad. Sci.* **113**, 7403–7407 (2016).
- W. Wróblewski and S. Dykas, “Two-fluid model with droplet size distribution for condensing steam flows,” *Energy* **106**, 112–120 (2016).
- P. M. Somwanshi, K. Muralidhar, and S. Khandekar, “Coalescence of vertically aligned drops over a superhydrophobic surface,” *Phys. Fluids* **32**, 052106 (2020).

- ⁵R. Blossey, "Self-cleaning surfaces—virtual realities," *Nat. Mater.* **2**, 301–306 (2003).
- ⁶Q. Vo and T. Tran, "Dynamics of droplets under electrowetting effect with voltages exceeding the contact angle saturation threshold," *J. Fluid Mech.* **925**, A19 (2021).
- ⁷R. Narhe, D. Beysens, and V. Nikolayev, "Contact line dynamics in drop coalescence and spreading," *Langmuir* **20**, 1213–1221 (2004).
- ⁸M. A. Nilsson and J. P. Rothstein, "The effect of contact angle hysteresis on droplet coalescence and mixing," *J. Colloid Interface Sci.* **363**, 646–654 (2011).
- ⁹J. Jin, C. H. Ooi, D. V. Dao, and N.-T. Nguyen, "Coalescence processes of droplets and liquid marbles," *Micromachines* **8**, 336 (2017).
- ¹⁰H. P. Kavehpour, "Coalescence of drops," *Annu. Rev. Fluid Mech.* **47**, 245–268 (2015).
- ¹¹A.-L. Biance, C. Clanet, and D. Quéré, "First steps in the spreading of a liquid droplet," *Phys. Rev. E* **69**, 016301 (2004).
- ¹²J. M. Ludwicki and P. H. Steen, "Sweeping by sessile drop coalescence," *Eur. Phys. J.: Spec. Top.* **229**, 1739–1756 (2020).
- ¹³J. M. Ludwicki, V. R. Kern, J. McCraney, J. B. Bostwick, S. Daniel, and P. H. Steen, "Is contact-line mobility a material parameter?," *npj Microgravity* **8**, 6 (2022).
- ¹⁴Y. Cheng, F. Wang, J. Xu, D. Liu, and Y. Sui, "Numerical investigation of droplet spreading and heat transfer on hot substrates," *Int. J. Heat Mass Transfer* **121**, 402–411 (2018).
- ¹⁵P. M. Somwanshi, V. Cheverda, K. Muralidhar, S. Khandekar, and O. Kabov, "Understanding vertical coalescence dynamics of liquid drops over a superhydrophobic surface using high-speed orthographic visualization," *Exp. Fluids* **63**, 47 (2022).
- ¹⁶J. Rose, "Dropwise condensation theory and experiment: A review," *Proc. Inst. Mech. Eng., Part A* **216**, 115–128 (2002).
- ¹⁷K. A. Estes and I. Mudawar, "Correlation of Sauter mean diameter and critical heat flux for spray cooling of small surfaces," *Int. J. Heat Mass Transfer* **38**, 2985–2996 (1995).
- ¹⁸M. Bao, F. Wang, Y. Guo, L. Gong, and S. Shen, "Experimental study of two-phase heat transfer of droplet impact on liquid film," *Phys. Fluids* **34**, 042119 (2022).
- ¹⁹Y.-H. Kim, B. Yoo, J. E. Anthony, and S. K. Park, "Controlled deposition of a high-performance small-molecule organic single-crystal transistor array by direct ink-jet printing," *Adv. Mater.* **24**, 497–502 (2012).
- ²⁰X. Gao, H. Chen, Q. Nie, and H. Fang, "Stability of line shapes in inkjet printing at low substrate speeds," *Phys. Fluids* **34**, 032002 (2022).
- ²¹M. A. Hack, P. Vondeling, M. Cornelissen, D. Lohse, J. H. Snoeijer, C. Diddens, and T. Segers, "Asymmetric coalescence of two droplets with different surface tensions is caused by capillary waves," *Phys. Rev. Fluids* **6**, 104002 (2021).
- ²²A. A. Saha and S. K. Mitra, "Effect of dynamic contact angle in a volume of fluid (VOF) model for a microfluidic capillary flow," *J. Colloid Interface Sci.* **339**, 461–480 (2009).
- ²³S. H. Davis, "Moving contact lines and rivulet instabilities. Part 1. The static rivulet," *J. Fluid Mech.* **98**, 225–242 (1980).
- ²⁴L. M. Hocking, "The damping of capillary-gravity waves at a rigid boundary," *J. Fluid Mech.* **179**, 253–266 (1987).
- ²⁵J. B. Bostwick and P. H. Steen, "Dynamics of sessile drops. Part 1. Inviscid theory," *J. Fluid Mech.* **760**, 5–38 (2014).
- ²⁶J. Zhang, P. Wang, M. K. Borg, J. M. Reese, and D. Wen, "A critical assessment of the line tension determined by the modified Young's equation," *Phys. Fluids* **30**, 082003 (2018).
- ²⁷W. Ren, D. Hu, and W. E, "Continuum models for the contact line problem," *Phys. Fluids* **22**, 102103 (2010).
- ²⁸H. Liu, J. Zhang, P. Capobianchi, M. K. Borg, Y. Zhang, and D. Wen, "A multi-scale volume of fluid method with self-consistent boundary conditions derived from molecular dynamics," *Phys. Fluids* **33**, 062004 (2021).
- ²⁹G. Amberg, "Detailed modelling of contact line motion in oscillatory wetting," *npj Microgravity* **8**, 1 (2022).
- ³⁰Y. Xia and P. H. Steen, "Moving contact-line mobility measured," *J. Fluid Mech.* **841**, 767–783 (2018).
- ³¹J. McCraney, V. Kern, J. Bostwick, S. Daniel, and P. Steen, "Oscillations of drops with mobile contact lines on the International Space Station: Elucidation of terrestrial inertial droplet spreading," *Phys. Rev. Lett.* **129**, 084501 (2022).
- ³²M. M. Weislogel and J. McCraney, "The symmetric draining of capillary liquids from containers with interior corners," *J. Fluid Mech.* **859**, 902–920 (2019).
- ³³J. McCraney, M. Weislogel, and P. Steen, "The draining of capillary liquids from containers with interior corners aboard the ISS," *npj Microgravity* **7**, 45 (2021).
- ³⁴J. Canny, "A computational approach to edge detection," *IEEE Trans. Pattern Anal. Mach. Intell.* **PAMI-8**, 679–698 (1986).
- ³⁵C. Kunkelmann, "Numerical modeling and investigation of boiling phenomena," Ph.D. thesis (Technische Universität, 2011).
- ³⁶J. Wasserfall, P. Figueiredo, R. Kneer, W. Rohlf, and P. Pischke, "Coalescence-induced droplet jumping on superhydrophobic surfaces: Effects of droplet mismatch," *Phys. Rev. Fluids* **2**, 123601 (2017).
- ³⁷J. Eggers, J. R. Lister, and H. A. Stone, "Coalescence of liquid drops," *J. Fluid Mech.* **401**, 293–310 (1999).
- ³⁸W. Ristenpart, P. McCalla, R. Roy, and H. A. Stone, "Coalescence of spreading droplets on a wettable substrate," *Phys. Rev. Lett.* **97**, 064501 (2006).
- ³⁹A. Menchaca-Rocha, A. Martínez-Dávalos, R. Nunez, S. Popinet, and S. Zaleski, "Coalescence of liquid drops by surface tension," *Phys. Rev. E* **63**, 046309 (2001).
- ⁴⁰D. Quéré, "Wetting and roughness," *Annu. Rev. Mater. Res.* **38**, 71–99 (2008).